Title: Illuminating the mystery of thylacine extinction: a role for relaxed selection and gene loss

Buddhabhushan Girish Salve, Nagarjun Vijay

Computational Evolutionary Genomics Lab, Department of Biological Sciences, IISER Bhopal, Bhauri, Madhya Pradesh, India

Author for Correspondence: Nagarjun Vijay, nagarjun@iiserb.ac.in

Abstract

Gene loss shapes lineage-specific traits but is often overlooked in species survival. In this study, we investigate the role of ancestral gene loss using the extinction icon─thylacine (*Thylacinus cynocephalus*). While studies of neutral genetic variation indicate a population decline before extinction, the impact of thylacine-specific ancestral gene losses remains unexplored. The availability of a chromosomal-level genome of the extinct thylacine offers a unique opportunity for such comparative studies. Here, we leverage palaeogenomic data to compare gene presence/absence patterns between the Tasmanian devil and thylacine. We discovered ancestral (an interval of 13-1 Ma) loss of *SAMD9L*, *HSD17B13*, *CUZD1* and *VWA7* due to multiple gene-inactivating mutations, corroborated by short-read sequencing. The timing of gene loss mirrors the thylacine's shift toward hypercarnivory and increased body size. Our genome-wide analysis reveals olfactory receptor loss and relaxed selection, aligning with reduced olfactory lobes in the thylacine, indicating olfaction is not its primary hunting sense. By integrating palaeogenomic data with comparative genomics, our study sheds light on ancestral gene losses and their impact on species fitness while providing a foundation for selecting candidate species and genes for thylacine de-extinction. Our approach can be extended to other extinct/endangered species, helping to identify genetic factors for de-extinction efforts.

Keywords

thylacine, extinct species, gene loss, RELAX selection, comparative genomics, de-extinction

1) Introduction

Traditional genetics-based approaches to species conservation have focused mainly on measures of genetic diversity, the prevalence of mutational load and recent demographic histories [1–7]. However, there has been little focus on ancestral gene loss and its potential role in species survival and extinction. This aspect remains underexplored in conservation genetics despite its potential impact on long-term species survival and resilience to rapid environmental changes due to anthropogenic activities. Several studies have shown that gene loss plays a key role in shaping phenotypic evolution [8,9], such as adaptations for blood-feeding in bats [10], modifications of the epidermis for aquatic environments in cetaceans [11], dietary variation and retention/pseudogenisation of *ADH7* [12,13] and loss of the *PLAAT1* gene in vertebrates for adaptation to low-light environments [14]. Nonetheless, ancestral gene losses have demonstrated implications for species survival. For instance, (i) the ancient loss of the *PON1* gene in marine mammals eliminates their primary defence against neurotoxicity from anthropogenic organophosphorus compounds, posing potential risks in modern environments [15], (ii) in odontocetes, the loss of *MX1* and *MX2* genes leads to decreased resistance to viral infections and long-term survival [16], and (iii) the loss of the *CNR2* gene makes parrots more susceptible to neuroinflammation [17], highlighting the consequences of gene loss in these species in terms of long-term survival and disease susceptibility. In previous studies, we highlighted that the loss of ciliary and immune cell genes contributes to differential susceptibility to influenza in bird species [18,19]. These findings emphasise that species-specific ancestral gene losses, which may have conferred advantages in adapting to unique environments in the distant past, can now have adverse effects in the present day because of anthropogenic activities [11] and underscore a critical link between gene loss and increased extinction risk.

As a promising approach, knowledge of gene losses in extinct species could provide valuable insights into the causes of species extinction, refine de-extinction strategies, and offer clues about evolutionary processes, such as trait evolvability. For example, the loss of the *FOXQ1* gene among extinct woolly mammoths has been linked to a reduced ability to adapt to cold climates, ultimately leading to lower fitness [20]. The advent of machine learning-based comparative genomics tools such as TOGA [21] and the increase in publicly available genomic data from both extant and extinct species make it possible to conduct genome-wide screening for ancestral gene loss in extinct species [21–25]. Gene loss can result from genetic drift, positive or relaxed selection, leading to exon deletions or the accumulation of mutations that disrupt the reading frame, such as premature stop codons, frameshifts, dysfunctional splice sites, or repeat insertions or chromosomal rearrangements [10,14,18,19,26,27]. The scarcity of multiple samples from extinct species hampers the robust estimation of genetic diversity and the prevalence of mutational load, making it challenging to fully understand their genetic dynamics and evolutionary history [28]. However, single-sample genomic data are sufficient for ancestral gene loss inference. Genome-wide screening for ancestral gene loss becomes vital when the only surviving species within a clade becomes extinct. For example, the thylacine (*Thylacinus cynocephalus*; also known as the Tasmanian tiger or Tasmanian wolf) was the largest modern-day carnivorous marsupial and the sole surviving member of the genus *Thylacinus* and the family *Thylacinidae* until modern times [29]. The *Thylacinidae* were small-bodied, generalist faunivores until the middle Miocene climatic transition (MMCT; ~15–13 Ma). Following this period, they increased in size and specialised in a hypercarnivorous diet [30]. This raises a critical question in conservation genetics: which genetic changes are unique to a species, and what are their functional impacts, particularly in terms of the species' long-term survivability, resilience to environmental changes, and vulnerability to novel diseases?

Thylacines were once widespread across continental Australia and New Guinea, but their disappearance from the mainland during the late Holocene was likely driven by climate change, human intensification, and competition with dingoes [31–33]. In Tasmania, however, thylacine numbers had already declined significantly by the early 1800s, following European settlement, the introduction of farming, a government hunting bounty, and disease, leading to eventual extinction, with the last recorded thylacine dying in 1936 [22,23,34]. However, mitochondrial and genomic DNA sequences suggest that limited genetic diversity in thylacine precedes climatic transition-mediated extinction [23,35,36]. Previous research has focused primarily on thylacine's canid-like craniofacial convergence, estimation of extinction date, phylogenetic relationships, demographic history, annotation of immune genes, genetic diversity, biology and anatomy [22,23,29,32,35,37–49].

In this study, we leverage paleogenomic data of thylacine to examine gene presence and absence patterns compared with the Tasmanian devil (*Sarcophilus harrisii*). We began with a genome-wide screen for gene losses in the thylacine, corroborating these loss events with short-read Illumina sequencing data. Additionally, we reconstructed the gene loss history using genomes from other marsupial species and assessed relaxed selection signatures. Our results offer novel insights into the ancestral loss of key genes in the thylacine, which may have influenced its extinction and environmental adaptations, providing a basis for refining genomics-informed genetic rescue strategies. Although the present study focuses on thylacine, our approach can easily be extended to other species and improve our understanding of species-specific biology, thereby refining de-extinction strategies.

2) Methods

(a) Genome-wide screen for thylacine-specific gene loss

We identified gene loss in the thylacine (*Thylacinus cynocephalus*) by comparing its genome to the Tasmanian devil (*Sarcophilus harrisii*). Firstly, using the make_lastz_chains v2.0.8 pipeline (https://github.com/hillerlab/make_lastz_chains), we created a pairwise chain-format genome alignment between the Tasmanian devil (GCF_902635505.1; chromosome-wise) and the thylacine assembly (GCA_007646695.3; whole genome). Next, we applied the machine learning-based tool TOGA v1.1.7 [21] to determine the status of genes in the thylacine genome, using the *-o2o_only* flag to include only genes with a single orthologous chain (see electronic supplementary material, figure S1).

(b) Reconstruction of gene loss history and its validation

We assessed the gene orthology of the gene loss candidates on the basis of their syntenic position within the genomes of human (*Homo sapiens*), opossum (*Monodelphis domestica*), yellow-footed antechinus (*Antechinus flavipes*) and Tasmanian devil (*Sarcophilus harrisii*) (see electronic supplementary material, table S1-S2). The gene-inactivating events inferred by TOGA for "clearly lost" genes were corroborated using the BLASTn v2.13.0 [50] search in ~223 Gb short-read data of thylacine (SRR5055303, SRR5055304, SRR5055305, and SRR5055306). The BLASTn results were manually inspected and confirmed, and IGV-reports v1.12.0 were used to visualise frame-disrupting events predicted by TOGA [51,52]. We also used bam-readcount v1.0.1 to obtain base-level support for the event at the specified position [53]. Additionally, cross-species mapping of thylacine short-read data to Tasmanian devil was done using Bowtie2 v2.5.4 [54], allowing multiple mismatches using the *--very-sensitive-local flag* [55]. We reassessed the whole-genome sequencing short-read data for the presence of in-frame stop codons using HybPiper v2.3.1 [12,56] and Patchwork [57]. To determine the integrity of the lost gene loci in the chromosomal-level assembly of the opossum (*Monodelphis domestica*), we used the *scan_alignment* and *alignment_plot* options of the klumpy tool [58] by supplying the bwa-mapped bam of the *HSD17B13* containing

chromosome (NC_077232.1) as an *alignment_map*. However, similar analyses could not be performed for the numbat (*Myrmecobius fasciatus*), coppery ringtail possum (*Pseudochirops cupreus*), plush-coated ringtail possum (*Pseudochirops corinnae*), and thylacine due to the unavailability of long-read sequencing data for these species.

To reconstruct the history of gene loss, we downloaded available chromosomal-level marsupial genomes from NCBI. In addition, we included scaffold-level assemblies of phylogenetically closely related species, such as numbat (*Myrmecobius fasciatus*) and fat-tailed dunnart (*Sminthopsis crassicaudata*) (n=21; see electronic supplementary material, table S3). The status of the lost genes (in thylacine and 20 other marsupials) was assessed using TOGA. For each transcript, TOGA was run on a subset of the genome identified using BLASTn. Briefly, a BLASTn search was conducted on marsupial genome assemblies using Tasmanian devil transcripts as queries. The resulting hits were processed using *mergeBed -d 10000* to merge close intervals and *slopBed -b 30000* to expand the regions on both sides. These regions were then extracted using *getFastaFromBed* of BEDTools v2.27.1 [59]. The resulting FASTA sequences were used to assess gene status with the TOGA pipeline. The phylogenetic tree for the marsupials was retrieved from the TimeTree website (https://timetree.org/) and used to identify shared gene loss events.

(c) Transcriptional status of lost genes

We investigated the RNA expression of the genes lost in thylacine using the publicly available Tasmanian devil and dunnart transcriptome sequencing data from 27 tissues (allantois, amnion, axillary nerve, bone marrow, brachial plexus nerve, brain stem, cerebellum, cerebrum, distal yolk sac, endometrium, eye, heart, liver, lung, optic nerve, ovary, oviduct, pancreas, prostate gland, proximal yolk sac, sciatic nerve, skin, spleen, testis, thyroid, trigeminal nerve and uterus) of both males and females. (BioProject ID:

PRJEB34650 [60] and PRJNA1028148 [61]; see electronic supplementary material, table S4). We obtained transcripts per million (TPM) values by performing pseudo-alignments of the reads to the longest isoforms of the Tasmanian devil and dunnart transcripts using kallisto v0.51.0 [62].

We also screened the expression status of the lost gene in the miRNA-seq database of thylacine using BLASTn. As a control, we queried the coding sequences of LOC100913894 (*ACTA*) and LOC100925998 (*MYH7*) [63]. Additionally, we assessed the transcriptional status of the *VWA7* gene using RNA-Seq data from the tongue, lung, and liver of the numbat (*Myrmecobius fasciatus*) [64].

(d) Evaluating the strength of selection, limitations with GC-content and estimation of gene loss timing

To test the relaxation of selection in gene loss candidates, we obtained pairwise codon alignments between the Tasmanian devil and other marsupials, including the thylacine from TOGA [21]. Codons affected by frameshifting insertions or deletions and premature stop codons were replaced by “NNN” to maintain a reading frame. A multiple sequence alignment (MSA) of the protein-coding sequence was done using PRANK v.170427 [65] in GUIDANCE2 v2.01 [66]. The sequence saturation in MSA was checked using the index to measure substitution saturation (Iss) proposed by Xia et al. [67], available in the DAMBE program. Furthermore, the alignments and phylogenetic tree obtained from the Timetree website (https://timetree.org/) were used to investigate whether the gene evolves under relaxed selection specifying one branch as the foreground and all other branches as background at a time in the RELAX model of the HyPhy program [68] and codeml of PAML program [69]. We also implemented aBSREL and BUSTED, which are branch and gene-wide tests, respectively, to test for signatures of selection on branches of the marsupial phylogeny

for the lost genes. Additionally, site-specific models such as FEL and MEME were used to identify sites evolving under positive and negative selection, and ggplot2 was used for visualisation in the R program [70]. We used the "fdr" method to adjust p-values for multiple species comparisons [71]. We quantified the magnitude of GC-biased gene conversion (gBGC) using MapNH v1.3.0 [72] and phastBias v1.6 [73].

The gene loss timing was estimated using the method proposed by Meredith et al. [74], which is based on two assumptions: (i) dS*f* = dS*p* (the synonymous substitution rate in the mixed branch (dS*f*) does not change after the gene is pseudogenised (dS*p*), i.e. the 1ds method), and (ii) dS*f* = 0.7 dS*p* (the synonymous substitution rate of a functional copy of the gene (dS*f*) is 0.7 times the substitution rate after pseudogenisation (dS*p*), i.e. the 2ds method). We used 38.5 Ma as the divergence time for the thylacine from its most recent common ancestor (MRCA) and dN/dS (ω) estimated for functional (ω*f*), mixed (ω*m*), and pseudogene (ω*p*) using a branch-free model in the codeml program from PAML using unrooted trees.

(e) *SAMD9* and *SAMD9L* gene phylogeny

To confirm that the *SAMD9* and *SAMD9L* sequences used are 1-to-1 orthologs, we evaluate the maximum likelihood tree generated from marsupial species' *SAMD9* and *SAMD9L* orthologs. Briefly, we created multiple sequence alignments using *SAMD9* and *SAMD9L* open reading frames (ORFs) using PRANK v.170427 [65] in GUIDANCE2 v2.01 [66]. Then, IQ-TREE was used to generate a gene tree with ultrafast bootstrap and SH-aLRT test using *-m MFP --alrt 1000 -B 1000 --boot-trees* flag [75–77]. We also calculated a concordance factor for each branch of the gene tree, comparing the gene tree computed from the complete MSA against the fraction of gene trees of the 1 kb window sequence.

3) Results

In brief, our comparative genomic analysis identified ancestral gene losses in the extinct thylacine, attributed to frame-disrupting changes and/or in-frame stop codons in synteny-confirmed orthologs of *SAMD9L*, *HSD17B13*, *CUZD1*, and *VWA7* (figure 1). Signatures of relaxed selection were detected in the thylacine lineage for *SAMD9*/*9L*, *CUZD1*, and *VWA7* genes using RELAX and/or codeml (see electronic supplementary material, table S5). The estimated timing of gene loss for these genes ranges from approximately 13-6 Ma (figure 2; see electronic supplementary material, table S6). Additionally, we observed rampant gene losses in olfactory receptor genes and other genes prone to pseudogenisation accompanied by signatures of relaxed selection (figure 3; see electronic supplementary material, table S1 and S5).

(a) Candidate Gene Losses: Identification and Validation

The thylacine genome was assembled using Illumina sequencing (HiSeq and NextSeq), which exhibits reduced coverage in regions with high GC content [22,23,78]. This limitation can lead to false positives in gene loss identification [79]. In our analysis, many genes categorised by TOGA as missing, partially intact, partially missing, uncertain loss, or clearly lost were associated with high GC content, low or no coverage, missing exons, or deleted exons (figure 3a; see electronic supplementary material, table S1 and figure S1). We filtered out gene loss candidates with high GC content, prevalence of G/C stretches, and insufficient coverage to minimise false positives, ensuring robust identification of true gene losses. Additionally, genes annotated as “Low-quality protein” in the Tasmanian devil genome were excluded, as they are potentially lost in the Tasmanian devil itself.

Furthermore, we observed widespread gene loss and signatures of relaxed selection in olfactory genes (figure 3b; see electronic supplementary material, table S1 and S5). These loci experience reduced purifying selection and evolve rapidly in many mammals, exhibiting

high rates of gene gain and loss [80,81]. Therefore, we did not pursue these findings further in our study. Also, we observe the loss of genes prone to pseudogenisation, such as *LOC100935028*, *PTCHD3*, and *LOC105749566* (see electronic supplementary material, table S1).

(b) Loss of *SAMD9L* and signatures of relaxed selection in *SAMD9/9L*

Our genome-wide analysis identified that *SAMD9L* is lost in the thylacine due to multiple gene-inactivating mutations. These mutations include the deletion of one base (A) at codon-287, an in-frame stop codon (CGA→TGA) at codon-511, a deletion of four bases (GGTG) between 1932-1937th position, an insertion of one base (C) at codon-667, and in-frame stop codons at codon-680 (CGA→TGA), codon-1207 (CAG→TAG), and codon-1463 (CAA→TAA) (figure 1). All seven events are supported by short-read sequencing data (see electronic supplementary material, figure S2). Further, HybPiper found non-terminal stop codons for *SAMD9L*, ruling out potential paralog-to-contig assignment errors. Among the screened marsupial genomes, *SAMD9L* loss was unique to the thylacine (figure 1), with an estimated timing of gene loss at approximately 11–8 Ma (figure 2; see electronic supplementary material, table S6). While other marsupial species such as the opossum, yellow-footed antechinus, and Tasmanian devil have intact *SAMD9L* genes with *TMPPE*, *CRTAP*, and *SUSD5* on the left flank, and *SAMD9*, *CDK6*, *FAM133B*, and *PEX1* on the right flank. In human *CALCR*, *VPS50* and *HEPACAM2* genes are on the left flank of *SAMD9L*, and *SAMD9*, *CDK6*, *FAM133B*, and *PEX1* genes are on the right flank (see electronic supplementary material, table S2). In addition to the synteny-based identification of *SAMD9L* orthologs, gene sequence-based phylogenetic trees also delineated the true orthologs with good bootstrap support (see electronic supplementary material, figure S3-S4). In the Tasmanian devil, *SAMD9L* is annotated as LOC100924681 (XM_031940019.1), with a GC content of 37.65%. The *SAMD9L* is expressed in the Tasmanian devil and dunnart lung,

ovary, and thyroid transcriptomes (figure 3c; see electronic supplementary material, table S4). Notably, we found signatures of relaxed selection using RELAX in *SAMD9* of the thylacine (p-value = 0.004; k-value = 0.16; figure 3b); in contrast, relaxed selection signatures are not found in closely related species of the *Dasyuridae* family. Additionally, we observed relaxed selection signatures for *SAMD9L* using codeml in PAML (see electronic supplementary material, table S5) and episodic diversifying positive selection using aBSREL (p-value = 0.00019) and BUSTED (p-value = 0.0061) models of the Hyphy program in thylacine. Some marsupial species of the *Macropodidae* family also exhibit signatures of relaxed selection (see electronic supplementary material, figure S5 and table S5).

The signatures of relaxed selection in *SAMD9*/*9L* and *SAMD9L* gene loss due to multiple gene-inactivating mutations indicate that thylacine may have become vulnerable to the critical function provided by *SAMD9* and *SAMD9L* genes. Interestingly, we found a loss of *SAMD9* in the orders Carnivora and Pholidota, while it remains intact in the closely related order Perissodactyla (see electronic supplementary material, figure S6).

(c) Loss of *HSD17B13*

In the thylacine, *HSD17B13* was inactivated through a splice-site mutation (gt →ga) at Exon1, and the deletion of one base (G) in Exon5 (figure 1c; see electronic supplementary material, figure S2). The estimated timing of this gene loss is approximately 2–1 Ma (figure 2; see electronic supplementary material, table S6). The Tasmanian devil's *HSD17B13* (XM_003774508.4) has a GC content of 39.98% and is expressed in the liver and pancreas (figure 3c; see electronic supplementary material, table S4). The micro-synteny of the human *HSD17B13* gene is flanked by *IBSP*, *DMP1*, *DSPP*, *SPARCL1*, *SCPPPQ1*, *NUDT9*, and *HSD17B11* on the left, while the right flank consists of *KLHL8*, *AFF1*, *C6H4orf36*, and

SLC10A6 genes. In the yellow-footed antechinus and Tasmanian devil, the left flank includes *IBSP*, *DMP1*, *DSPP*, *NUDT9*, and *HSD17B11*, while the right flank remains consistent with humans, containing *KLHL8*, *AFF1*, *C6H4orf36*, and *SLC10A6* (see electronic supplementary material, table S2).

Notably, *HSD17B13* annotation is missing from the annotated genome of the opossum in the NCBI Genome Data Viewer (see electronic supplementary material, figure S7). We found that *HSD17B13* is independently lost in opossum due to an in-frame stop codon (TGG → TGA) in Exon1 (polymorphic blastn hits found for this event) and deletion of Exons 3-to-7 (figure 1b, see electronic supplementary material, figure S7). We identified an assembly gap at the syntenic locus (see electronic supplementary material, figure S8); however, a BLASTn search in the long-read database returned spurious hits for Exons 3-to-7. Additionally, signatures of relaxed selection were found in the opossum using RELAX (p-value = 0.0008; k-value = 0.00) and PAML's codeml (see electronic supplementary material, table S5). At the same time, episodic diversifying positive selection was detected in the opossum's *HSD17B13* using aBSREL (p-value = 0.00) and BUSTED (p-value = 0.00) models (see electronic supplementary material, table S5).

(d) Loss of *CUZD1*

We identified multiple gene-inactivating mutations in *CUZD1* that contributed to its loss in thylacine (figure 1c). These include the deletion of one base (G) at codons-67 and 95, an in-frame stop codon (TAC → TAG) at codon-119, and another premature stop codon (TGC → TGA) at codon-283 (see electronic supplementary material, figure S2). Furthermore, BLASTn analysis recovered only partial sequences for Exon6, whereas no BLASTn hits were obtained for Exons 7-8, indicating its likely deletion. The estimated timing of gene loss is approximately 13-9 Ma (figure 2). The *CUZD1* gene, annotated as LOC100927202

(XM_003755291.4) in the Tasmanian devil, has a GC content of 39.35% and is expressed in the pancreas (figure 3c; see electronic supplementary material, table S4). Notably, we found signatures of relaxed selection by the PAML codeml. At the same time, we found evidence for intensification by RELAX model (p-value = 0.00; k-value = 3.72) and signatures of episodic diversifying positive selection are detected in thylacine *CUZD1* by aBSREL (p-value = 0.00) and BUSTED (p-value = 0.00) models of Hyphy (see electronic supplementary material, table S5). Additionally, *CUZD1* independently lost in the golden ringtail possum (*Pseudochirops corinnae*) and the coppery ringtail possum *(Pseudochirops cupreus*); both species belong to the marsupial family *Pseudocheiridae*. In golden ringtail possum, no BLASTn hits were found for Exons 1-to-4 in the genomic short-read database, while Exon5 exhibited two in-frame stop codons (CAA → TAA and TCA → TGA) and one base (A) deletion. In coppery ringtail possum, an in-frame stop codon (CAA → TAA) and one base (A) deletion led to the inactivation of *CUZD1* (figure 1b; see electronic supplementary material, figure S9). Two gene-inactivating mutations in Exon5 of these two species are shared. At the same time, this gene remains intact in the western ringtail possum (*Pseudocheirus occidentalis*), suggesting that *CUZD1* was lost independently within the *Pseudochirops* genus at approximately 25-20 Ma.

Our micro-syntenic analysis found that in humans, *KZF5*, *PSTK*, *LOC124902519*, C10orf88B, and *FAM24B* genes occur on the left flank of *CUZD1* and LOC124900290, *DMBT1L1*, and *SPADHI* on the right flank. However, among marsupials (opossum, yellow-footed antechinus and Tasmanian devil), the right flank has C2H10orf88, *PSTK*, and *IKZF5*, whereas, on the left flank, *HTRA1* and *DMBT1* were annotated in the NCBI genome data viewer and located approximately 350 kb away (see electronic supplementary material, table S2).

(e) Loss of G7c (*VWA7*)

This gene has acquired multiple gene-inactivation mutations in thylacine (figure 1c). Insertion of one base (C) in codon-37, two base deletion of CA in codon-171, insertion of one base (T) at codon-403, TGG → TAG premature stop codon at codon-575 and insertion of two bases (TA) leading to an in-frame stop codon (GCC → TAG) at codon-706 (see electronic supplementary material, figure S2). The estimated timing of gene loss is approximately 8-6 Ma (figure 2). The GC content of Tasmanian devil *VWA7* (XM_003768930.3) is 51.71 % and expressed in the dunnart oviduct (figure 3; see electronic supplementary material, table S4). The micro-synteny of *VWA7* in humans includes *HSPA1A*, *HSPA1L*, *LSM2*, and *VARS1* on the left flank, whereas *SAPCD1*, *MSH5*, *CLIC1*, and *DAH2* are on the right flank. A similar gene arrangement flanked *VWA7* in marsupials such as the opossum, yellow-footed antechinus, and Tasmanian devil (see electronic supplementary material, table S2). We found that *VWA7* is lost in numbat due to an in-frame stop codon in Exon5 and Exon14 and the deletion of one base in Exon14 (figure 1, also see electronic supplementary material, figure S10). We found signatures of relaxed selection by RELAX (p-value = 0.01; k-value = 0.40) as well as by codeml in thylacine, and lack of expression at its syntenic locus, suggesting *VWA7* gene loss in numbat (see electronic supplementary material, table S4-S5 and figure S11).

4) Discussion

In this study, we used thylacine, an extinction icon, as a case study to investigate ancestral gene losses through a comparative genomic approach. Our genome-wide comparative study between the Tasmanian devil and thylacine identified the ancestral gene loss of *SAMD9L*, *HSD17B13*, *CUZD1*, *VWA7* and several olfactory receptors. Short-read sequencing confirmed all gene-inactivating mutations, validating gene loss in the thylacine. Our investigation into the timing of gene losses reveals a staggered pattern spanning approximately 13-1 Ma. Notably, the genes lost in the thylacine neither exhibit recurrent loss across the marsupial

species screened nor pervasive signatures of relaxed selection. The signatures of relaxed selection detected by RELAX and/or codeml for the lost genes, along with estimated dN/dS values for functional branches, are consistently lower than those for mixed branches, which is consistent with the hypothesis that the lost genes evolved under progressively more relaxed constraints (see electronic supplementary material, table S5- S7) [74,82]. This finding suggests that the loss of these genes was not a common evolutionary occurrence within marsupials and likely reflects unique selective pressures or stochastic events in the thylacine lineage. The genes lost in thylacine are expressed in comparable tissues in the Tasmanian devil and dunnart transcriptomes, indicating that they have a conserved functional role [83]. These genes have conserved functions across mammals, but their roles may vary between species. The functions of the lost genes provide valuable insights into their potential impact on thylacine biology. For instance, these genes play roles in antiviral defence, metabolic processes, lactation signalling pathways, pancreatitis and tumour susceptibility. The loss of these genes may have influenced the fitness of thylacine, potentially making it more susceptible to diseases and/or reducing its adaptive capacity. Such vulnerabilities might have contributed to its extinction. From a broader perspective, these findings have significant implications for conservation genomics and de-extinction initiatives. Understanding the functional roles of lost genes can inform genome editing strategies aimed at resurrecting extinct species. Specifically, pinpointing and targeting these loci can aid in selecting suitable candidate species and genes for genome editing, thereby enhancing the feasibility and success of de-extinction projects.

(a) Impact of ancestral gene losses on thylacine fitness and adaptation

The thylacine genome exhibits the loss of four genes- *SAMD9L*, *HSD17B13*, *CUZD1*, and *VWA7* -each with important biological functions and implications for species fitness. Our investigation into the timing of gene loss events revealed a staggered pattern, occurring over

a span of approximately 13-1 Ma. This temporal distribution indicates that the gene losses were not confined to a single evolutionary event but occurred progressively after the MMCT. The *SAMD9L* (Sterile Alpha Motif Domain Containing 9 Like) is a paralog of *SAMD9* [84]. The *SAMD9*/*9L* genes are critical antiviral factors and tumour suppressors, playing crucial roles in the innate immune defence against poxviruses, HIV-1 and lentivirus [85–87]. The *SAMD9* gene is lost (deleted) in the mouse due to evolutionary genomic rearrangements [84,88], and mouse *SAMD9L* is not a functional paralog of human *SAMD9* [89]. Notably, species-specific differences in *SAMD9L* among rodents act as a natural barrier to cross-species orthopoxvirus infections, underscoring the adaptive significance of these genes in shaping immune defences across different lineages [90]. Furthermore, SAMD9L is the only gene that experienced convergent amino acid substitutions and an accelerated evolutionary shift among bats and birds, which are natural hosts of several zoonotic pathogens, highlighting its crucial role in conferring resistance to viruses [91]. Our study found that *SAMD9* and *SAMD9L* are highly conserved across marsupials, except for thylacine. Hence, the loss of *SAMD9L* indicates the possibility of increased vulnerability to zoonotic viral infections and compromised immune responses in thylacine. Another lost gene, *HSD17B13* (Hydroxysteroid 17-beta-dehydrogenase 13), encodes a hepatic lipid droplet-associated enzyme [92]. Loss-of-function variants in *HSD17B13* are associated with protection against the progression of steatosis to more severe liver conditions [93], suggesting that *HSD17B13* gene loss could have functional adaptive significance. The CUB and zona pellucida-like domain-containing protein 1 (*CUZD1*) is also lost in the thylacine. *CUZD1* interacts with *JAK1*/*JAK2* and *STAT5*, which are mediators of prolactin signalling critical for mammary gland development. Its absence abolishes *STAT5* phosphorylation during amelogenesis, leading to defective lactation [94]. Furthermore, *CUZD1* is abundantly expressed in pancreas acinar cells of human and mouse [95,96]. We also found that *CUZD1* is expressed in the

Tasmanian devil's pancreas. *CUZD1* deficient mice demonstrated increased severity of experimentally induced acute pancreatitis, suggesting *CUZD1* is a strong candidate as a pancreatitis susceptibility gene [96,97]. Finally, *VWA7* (Von Willebrand Factor A Domain Containing 7), also known as G7c, is located in the mouse and human MHC class III region [98]. The *VWA7* gene has been implicated in controlling lung tumour susceptibility and host immune response to viral infections, suggesting its potential role in disease susceptibility [99–102].

Interestingly, the timing of gene losses for *SAMD9L*, *CUZD1*, and *VWA7* is estimated to be approximately 13–6 Ma, a period that follows the middle Miocene climatic transition (MMCT; ~15–13 Ma). This period marked significant ecological and climatic changes, during which *Thylacinidae*, previously small-bodied, unspecialised faunivores, began to undergo notable shifts. After MMCT, they increased in size and developed adaptations to a hypercarnivorous diet, likely driven by aridification of the Australian environment [30,103]. Notably, gene loss has also been observed during major evolutionary transitions, such as from unicellular to multicellular life and from land to water [104,105].

In addition, our analysis revealed a drastic loss of olfactory receptors in the thylacine, paired with relaxed selection, aligning with earlier findings of its reduced olfactory lobes [30,106]. Unlike the Tasmanian Devil, a scavenger, the taller thylacine likely depended on vision and sound for hunting, aided by its ability to see over vegetation. This shift in sensory reliance is further evidenced by the pronounced ridges on its neocortex, suggesting heightened cognitive abilities to support its hunting strategies [107]. Besides this, the thylacine and grey wolf exemplify remarkable convergent evolution, displaying strikingly similar craniofacial morphologies despite ~160 million years of evolutionary divergence [22,23]. Our study identified the convergent loss of *SAMD9L* in the thylacine and *SAMD9* in carnivores and pangolins while it is intact in Perissodactyla, highlighting potential links to dietary

adaptations. Notably, these genes are located near a candidate craniofacial cis-regulatory element, indicating a possible connection with phenotypic convergence (see supplementary table of [108]). This pattern underscores the complexity of gene loss events and their potential role in shaping convergent phenotypic traits, which remains to be verified experimentally [109].

Whatever the cause for gene loss, the loss of *SAMD9L*, *HSD17B13*, *CUZD1*, and *VWA7* genes in the thylacine possibly had negative pleiotropic effects, potentially compromising its health by affecting antiviral defence, metabolic processes, lactation, pancreatitis and tumour susceptibility. At the same time, adaptive ancestral gene loss may have provided specific advantages to the thylacine in response to environmental pressures. Model-based population viability analyses suggest that the disease played only a minor role in thylacine extinction [110]. Simultaneously, other studies suggest that a 'canine-distemper-like' disease played a role in exacerbating its extinction [45,111,112].

(b) Studying gene loss in extinct species: Opportunities, constraints, and conservation implications

Comparative studies of extinct species offer valuable insights into host-specific immune responses and phenotypic evolution [8,18]. Such studies can play a pivotal role in refining de-extinction strategies by assisting in selecting candidate species and genetic loci for genome editing, thereby informing decisions about diet and habitat preferences [113–115]. Advances in comparative genomics, powered by the availability of numerous sequenced genomes, tools and recent breakthroughs in sequencing technologies to sequence ancient samples, enable researchers to connect genomic variations—such as the loss of ancestral protein-coding genes—with phenotypic diversity [11,21,24,25,116]. These insights help uncover the molecular mechanisms driving the evolution of species, highlight potential risks to modern

environments, and illuminate the factors influencing species survival [15–17,20]. Gene loss identification heavily depends on the quality of genome assemblies [10]. For extinct species, sequencing is generally performed using Illumina technology [22], which has known limitations in sequencing GC-rich regions, potentially resulting in false positives for gene loss [79]. The fragmentary nature of ancient DNA in such species further restricts the use of long-read sequencing technologies [117]. This lack of long-read sequencing and the absence of transcriptomic data make it even more challenging to differentiate between assembly artefacts and true gene losses. However, recent breakthroughs in sequencing technologies, such as PaleoHi-C, are driving advancements in this field [118]. It is also possible that DNA damage in ancient specimens contributes to some of the observed stop codons [20].

Specifically for thylacine, the genome assembly (GCA_007646695.3) was assembled using Illumina HiSeq and NextSeq platforms. In line with previous research, our study finds that genes with high GC content tend to have lower sequencing coverage [79,119] and, therefore, are classified as missing, partially intact, or partially lost by TOGA. As a result, this might lead to incomplete or less reliable assemblies in GC-rich genomic regions, affecting the accuracy of downstream analyses and may lead to false positives for gene loss [79]. The lack of long-read sequencing (e.g., PacBio or Nanopore) limits genome assembly verification, and the absence of transcriptomic data (RNA-Seq) prevents the confirmation of gene loss at the expression level. Since the genome assembly is derived from a female thylacine, the Y chromosome has not been sequenced, restricting analyses to autosomes (1–6) and the X chromosome. Although miRNA-Seq data is available [63], it does not provide insights into protein-coding gene expression. Cytosine deamination and depurination could affect assembly integrity, potentially causing false gene loss, but studies suggest only minor depurination effects [22]. The gene losses we identified involve gene-inactivating mutations (e.g., splice-site changes, stop codons, insertions, and deletions) supported by forward and

reverse short reads, indicating they are genuine rather than artefacts of ancient DNA damage. Future improvements to the thylacine genome assembly will strengthen the assertion of gene losses.

Although habitat loss, hunting, introduced species, inbreeding depression, and loss of genetic diversity are widely recognised as key contributors to species extinction [2,120], these factors have primarily dominated conservation genetics studies focused on mitigating risks to threatened species [3,5,6,121]. In contrast, the role of ancestral gene loss in species extinction remains largely unexplored. Insights into ancestral lineage-specific gene losses can deepen our understanding of extinct species evolution and refine de-extinction approaches. Our study also offers a framework to test hypotheses on why specialist phylogenetic lineages struggle to persist and diversify [11,122] and provides a novel perspective on the interplay between species diversity and genetic diversity [123].

5) Conclusion

Our study offers an immediate framework that includes practical approaches in comparative genomics and insights into de-extinction strategies. Our findings from this case study of an extinction icon- the thylacine─establishes the ancestral gene loss of *SAMD9L*, *HSD17B13*, *CUZD1*, and *VWA7*, contributing unique insights into the genetic factors influencing extinction. Additionally, we observe gene loss in olfactory receptors and genes prone to pseudogenisation, such as *LOC100935028*, *PTCHD3*, and LOC105749566.

In line with temporal estimations of gene losses, our study provides an empirical case where we observe the coincidence of gene loss timing (approximately 13–6 Ma, following the middle Miocene climatic transition ~15–13 Ma). This period marked significant ecological and climatic changes, during which *Thylacinidae*, previously small-bodied, unspecialised faunivores, underwent notable shifts such as an increase in size and developing adaptations to

a hypercarnivorous diet, likely driven by the aridification of the Australian environment [30,103]. As the thylacine was the only surviving member of the genus *Thylacinus* and the family *Thylacinidae* until modern times, our study also offers a hypothesis on why specialist phylogenetic lineages struggle to persist and diversify over macroevolutionary timescales [11,29,122]. The genes lost in the thylacine did not show recurrent loss across other marsupial species or signs of relaxed selection, indicating that their loss was likely due to unique selective pressures or stochastic events in the thylacine lineage. Furthermore, our analysis reveals a pervasive loss of olfactory receptors in the thylacine, reflecting relaxed selection and correlating with its reduced olfactory lobes. This shift in sensory reliance, possibly driven by changes in traits such as height and vision, contrasts with that of the Tasmanian devil.

In addition, our analysis provides critical information for identifying which species are better candidates for cloning and which genetic loci are suitable for genome editing, contributing to future de-extinction efforts for thylacine and guiding decisions about diet and habitat preferences [113–115]. Our study provides a framework for identifying ancestral gene losses that may improve the probability of success of de-extinction programs.

Ethics

This work did not require ethical approval from a human subject or animal welfare committee.

Data accessibility

The data and relevant code for this study are available on GitHub: https://github.com/CEGLAB-Buddhabhushan/Thylacine_Genome-wide_GENELOSS.git

Declaration of AI use

We have not used AI-assisted technologies to create this article.

Authors' contributions

B.G.S.: conceptualisation, data curation, formal analysis, investigation, methodology, validation, visualisation, writing—original draft, writing—review and editing; N.V.: conceptualisation, funding acquisition, supervision, investigation, methodology, validation, writing—original draft, writing — review, and editing.

All authors gave final approval for publication and agreed to be held accountable for the work performed therein.

Funding

This article was funded by the Department of Biotechnology, Ministry of Science and Technology, India (grant no. BT/11/IYBA/2018/03) and Science and Engineering Research Board (grant no. ECR/2017/001430) provided funds for procuring computational resources (i.e. Har Gobind Khorana Computational Biology cluster) used.

Conflict of interest declaration

We declare that we have no competing interests.

Acknowledgements

We thank the Council of Scientific & Industrial Research for a fellowship to B.G.S. We used BioRender (https://biorender.com) to arrange figures and images of species. We thank Sandhya Sharma for the animal paintings in Figure 1.

References

1. Bouzat JL. 2010 Conservation genetics of population bottlenecks: the role of chance, selection, and history. *Conserv Genet* **11**, 463–478. (doi:10.1007/s10592-010-0049-0)

2. Frankham R. 2005 Genetics and extinction. *Biol Conserv* **126**, 131–140. (doi:10.1016/j.biocon.2005.05.002)

3. Khan A *et al.* 2021 Genomic evidence for inbreeding depression and purging of deleterious genetic variation in Indian tigers. *Proc. Natl. Acad. Sci. U. S. A.* **118**, e2023018118. (doi:10.1073/PNAS.2023018118/SUPPL_FILE/PNAS.2023018118.SAPP.PDF)

4. Patil AB, Vijay N. 2023 Conservation implications of diverse demographic histories: the case study of green peafowl (Pavo muticus, Linnaeus 1766). *Conserv. Genet.* , 1–14. (doi:10.1007/S10592-023-01580-9/FIGURES/4)

5. Pinto A V., Hansson B, Patramanis I, Morales HE, van Oosterhout C. 2023 The impact of habitat loss and population fragmentation on genomic erosion. *Conserv. Genet.* **25**, 49–57. (doi:10.1007/S10592-023-01548-9/FIGURES/3)

6. Willi Y, Kristensen TN, Sgro CM, Weeks AR, Ørsted M, Hoffmann AA. 2022 Conservation genetics as a management tool: the five best-supported paradigms to assist the management of threatened species. *PNAS* **119**, e2105076119. (doi:10.1073/pnas.2105076119)

7. Bell DA, Kovach RP, Whiteley AR. 2024 Inbreeding avoidance and cost in a small, isolated trout population. *Proc. B* **291**. (doi:10.1098/RSPB.2024.1164)

8. Albalat R, Cañestro C. 2016 Evolution by gene loss. *Nat. Rev. Genet. 2016 177* **17**, 379–391. (doi:10.1038/nrg.2016.39)

9. Guijarro-Clarke C, Holland PWH, Paps J. 2020 Widespread patterns of gene loss in the evolution of the animal kingdom. *Nat. Ecol. Evol. 2020 44* **4**, 519–523. (doi:10.1038/s41559-020-1129-2)

10. Blumer M *et al.* 2022 Gene losses in the common vampire bat illuminate molecular adaptations to blood feeding. *Sci. Adv.* **8**, 6494. (doi:10.1126/SCIADV.ABM6494/SUPPL_FILE/SCIADV.ABM6494_TABLES_S1_TO_S5.ZIP)

11. Sharma V, Hecker N, Roscito JG, Foerster L, Langer BE, Hiller M. 2018 A genomics approach reveals insights into the importance of gene losses for mammalian adaptations. *Nat. Commun. 2018 91* **9**, 1–9. (doi:10.1038/s41467-018-03667-1)

12. Pinto SL *et al.* 2023 Diet and the evolution of *ADH7* across seven orders of mammals. *R. Soc. Open Sci.* **10**. (doi:10.1098/RSOS.230451)

13. Janiak MC, Pinto SL, Duytschaever G, Carrigan MA, Melin AD. 2020 Genetic evidence of widespread variation in ethanol metabolism among mammals: revisiting the 'myth'' of natural intoxication'. *Biol. Lett.* **16**. (doi:10.1098/RSBL.2020.0070)

14. Drabeck DH *et al.* 2024 Gene loss and relaxed selection of plaat1 in vertebrates adapted to low-light environments. *Proc. R. Soc. B* **291**. (doi:10.1098/RSPB.2023.2847)

15. Meyer WK *et al.* 2018 Ancient convergent losses of Paraoxonase 1 yield potential risks for modern marine mammals. *Science (80-.).* **361**, 591–594. (doi:10.1126/SCIENCE.AAP7714/SUPPL_FILE/AAP7714_TABLES9.XLSX)

16. Braun BA, Marcovitz A, Camp JG, Jia R, Bejerano G. 2015 Mx1 and Mx2 key antiviral proteins are surprisingly lost in toothed whales. *Proc. Natl. Acad. Sci. U. S. A.* **112**, 8036–8040. (doi:10.1073/PNAS.1501844112/SUPPL_FILE/PNAS.201501844SI.PDF)

17. Divín D *et al.* 2022 Cannabinoid receptor 2 evolutionary gene loss makes parrots more

susceptible to neuroinflammation. *Proc. R. Soc. B* **289**. (doi:10.1098/RSPB.2022.1941)

18. Salve BG, Kurian AM, Vijay N. 2023 Concurrent loss of ciliary genes WDR93 and CFAP46 in phylogenetically distant birds. (doi:10.1098/rsos.230801)

19. Salve BG, Sharma S, Vijay N. 2024 Evolutionary diversity of CXCL16-CXCR6: Convergent substitutions and recurrent gene loss in sauropsids. *Immunogenet. 2024 765* **76**, 397–415. (doi:10.1007/S00251-024-01357-5)

20. Rogers RL, Slatkin M. 2017 Excess of genomic defects in a woolly mammoth on Wrangel island. *PLoS Genet.* **13**, e1006601. (doi:10.1371/journal.pgen.1006601)

21. Kirilenko BM *et al.* 2023 Integrating gene annotation with orthology inference at scale. *Science (80-.).* **380**. (doi:10.1126/science.abn3107)

22. Feigin CY *et al.* 2018 Genome of the Tasmanian tiger provides insights into the evolution and demography of an extinct marsupial carnivore. *Nat. Ecol. Evol.* **2**, 182–192. (doi:10.1038/s41559-017-0417-y)

23. Feigin C, Frankenberg S, Pask A. 2022 A Chromosome-Scale Hybrid Genome Assembly of the Extinct Tasmanian Tiger (Thylacinus cynocephalus). *Genome Biol. Evol.* **14**. (doi:10.1093/GBE/EVAC048)

24. Koepfli KP *et al.* 2015 The Genome 10K Project: a way forward. *Annu. Rev. Anim. Biosci.* **3**, 57–111. (doi:10.1146/ANNUREV-ANIMAL-090414-014900)

25. Rhie A *et al.* 2021 Towards complete and error-free genome assemblies of all vertebrate species. **592**, 737–746. (doi:10.1038/s41586-021-03451-0)

26. Sharma A, Gupta S, Patil AB, Vijay N. 2022 Birth and death in terminal complement pathway. *Mol. Immunol.* **149**, 174–187. (doi:10.1016/J.MOLIMM.2022.07.006)

27. Shinde SS, Sharma S, Teekas L, Sharma A, Vijay N. 2021 Recurrent erosion of COA1/MITRAC15 exemplifies conditional gene dispensability in oxidative phosphorylation. *Sci. Reports 2021 111* **11**, 1–16. (doi:10.1038/s41598-021-04077-y)

28. Dutoit L, Vijay N, Mugal CF, Bossu CM, Burri R, Wolf J, Ellegren H. 2017 Covariation in levels of nucleotide diversity in homologous regions of the avian genome long after completion of lineage sorting. *Proc. R. Soc. B Biol. Sci.* **284**. (doi:10.1098/RSPB.2016.2756)

29. Krajewski C, Driskell AC, Baverstock PR, Braun MJ. 1992 Phylogenetic relationships of the thylacine (Mammalia: Thylacinidae) among dasyuroid marsupials: Evidence from cytochrome b DNA sequences. *Proc. R. Soc. B Biol. Sci.* **250**, 19–27. (doi:10.1098/rspb.1992.0125)

30. Rovinsky DS, Evans AR, Adams JW. 2019 The pre-Pleistocene fossil thylacinids (Dasyuromorphia: Thylacinidae) and the evolutionary context of the modern thylacine. *PeerJ* **2019**, 1–41. (doi:10.7717/peerj.7457)

31. Letnic M, Fillios M, Crowther MS. 2012 Could direct killing by larger dingoes have caused the extinction of the thylacine from mainland Australia? *PLoS One* **7**, 19–23. (doi:10.1371/journal.pone.0034877)

32. White LC, Mitchell KJ, Austin JJ. 2018 Ancient mitochondrial genomes reveal the demographic history and phylogeography of the extinct, enigmatic thylacine (Thylacinus cynocephalus). *J. Biogeogr.* **45**, 1–13. (doi:10.1111/jbi.13101)

33. White LC, Saltré F, Bradshaw CJA, Austin JJ. 2018 High-quality fossil dates support a synchronous, Late Holocene extinction of devils and thylacines in mainland Australia. *Biol. Lett.* **14**, 10–13. (doi:10.1098/rsbl.2017.0642)

34. Gough N. 2001 Robert Paddle 2000, The Last Tasmanian Tiger: The History and Extinction of the Thylacine. Cambridge University Press, Oakleigh, Victoria. *Aust. J. Environ. Educ.* **17**, 162–163. (doi:10.1017/S0814062600003670)

35. Menzies BR, Renfree MB, Heider T, Mayer F, Hildebrandt TB, Pask AJ. 2012 Limited genetic diversity preceded extinction of the Tasmanian tiger. *PLoS One* **7**. (doi:10.1371/journal.pone.0035433)

36. Miller W *et al.* 2012 Polar and brown bear genomes reveal ancient admixture and demographic footprints of past climate change. *Proc. Natl. Acad. Sci. U. S. A.* **109**, E2382–E2390. (doi:10.1073/PNAS.1210506109/SUPPL_FILE/SAPP.PDF)

37. Old JM. 2015 Immunological insights into the life and times of the extinct tasmanian tiger (Thylacinus cynocephalus). *PLoS One* **10**, 1–17. (doi:10.1371/journal.pone.0144091)

38. Newton AH, Weisbecker V, Pask AJ, Hipsley CA. 2021 Ontogenetic origins of cranial convergence between the extinct marsupial thylacine and placental gray wolf. *Commun. Biol.* **4**, 1–9. (doi:10.1038/s42003-020-01569-x)

39. Miller W *et al.* 2009 The mitochondrial genome sequence of the Tasmanian tiger [Thylacinus cynocephalus]. *Genome Res.* **19**, 213–220. (doi:10.1101/gr.082628.108)

40. Brook BW, Sleightholme SR, Campbell CR, Buettel JC. 2018 Deficiencies in estimating the extinction date of the thylacine with mixed certainty data. *Conserv. Biol.* **32**, 1195–1197. (doi:10.1111/cobi.13186)

41. Wroe S, Clausen P, McHenry C, Moreno K, Cunningham E. 2007 Computer simulation of feeding behaviour in the thylacine and dingo as a novel test for convergence and niche overlap. *Proc. R. Soc. B Biol. Sci.* **274**, 2819–2828.

(doi:10.1098/rspb.2007.0906)

42. Pask AJ, Behringer RR, Renfree MB. 2008 Resurrection of DNA function in vivo from an extinct genome. *PLoS One* **3**, 3–7. (doi:10.1371/journal.pone.0002240)

43. Peel E, Frankenberg S, Hogg CJ, Pask A, Belov K. 2021 Annotation of immune genes in the extinct thylacine (Thylacinus cynocephalus). *Immunogenetics* **73**, 263–275. (doi:10.1007/s00251-020-01197-z)

44. Rovinsky DS, Evans AR, Martin DG, Adams JW. 2020 Did the thylacine violate the costs of carnivory? Body mass and sexual dimorphism of an iconic Australian marsupial. *Proc. R. Soc. B Biol. Sci.* **287**. (doi:10.1098/rspb.2020.1537)

45. Carlson CJ, Bond AL, Burgio KR. 2018 Estimating the extinction date of the thylacine with mixed certainty data. *Conserv. Biol.* **32**, 477–483. (doi:10.1111/cobi.13037)

46. Haines E, Bailey E, Nelson J, Fenlon LR, Suárez R. 2023 Clade-specific forebrain cytoarchitectures of the extinct Tasmanian tiger. *Proc. Natl. Acad. Sci. U. S. A.* **120**. (doi:10.1073/PNAS.2306516120)

47. Janis CM, Figueirido B. 2014 Forelimb anatomy and the discrimination of the predatory behavior of carnivorous mammals: The thylacine as a case study. *J. Morphol.* **275**, 1321–1338. (doi:10.1002/jmor.20303)

48. Figueirido B, Janis CM. 2011 The predatory behaviour of the thylacine: Tasmanian tiger or marsupial wolf? *Biol. Lett.* **7**, 937–940. (doi:10.1098/rsbl.2011.0364)

49. Newton AH, Spoutil F, Prochazka J, Black JR, Medlock K, Paddle RN, Knitlova M, Hipsley CA, Pask AJ. 2018 Letting the ‘cat’ out of the bag: Pouch young development of the extinct tasmanian tiger revealed by X-ray computed tomography. *R. Soc. Open Sci.* **5**. (doi:10.1098/rsos.171914)

50. Camacho C, Coulouris G, Avagyan V, Ma N, Papadopoulos J, Bealer K, Madden TL. 2009 BLAST+: architecture and applications. *BMC Bioinformatics* **10**, 421. (doi:10.1186/1471-2105-10-421)

51. Thorvaldsdottir H, Robinson JT, Mesirov JP. 2013 Integrative Genomics Viewer (IGV): high-performance genomics data visualization and exploration. *Brief. Bioinform.* **14**, 178–192. (doi:10.1093/bib/bbs017)

52. Rangwala SH *et al.* 2021 Accessing NCBI data using the NCBI Sequence Viewer and Genome Data Viewer (GDV). *Genome Res.* **31**, 159–169. (doi:10.1101/GR.266932.120)

53. Khanna A *et al.* 2022 Bam-readcount - rapid generation of basepair-resolution sequence metrics. *ArXiv* **7**, 3722. (doi:10.21105/joss.03722)

54. Langmead B, Salzberg SL. 2012 Fast gapped-read alignment with Bowtie 2. *Nat. Methods 2012 94* **9**, 357–359. (doi:10.1038/nmeth.1923)

55. Gershman A *et al.* 2023 Genomic insights into metabolic flux in hummingbirds. *Genome Res.* **33**, 703–714. (doi:10.1101/GR.276779.122/-/DC1)

56. Johnson MG, Gardner EM, Liu Y, Medina R, Goffinet B, Shaw AJ, Zerega NJC, Wickett NJ. 2016 HybPiper: Extracting coding sequence and introns for phylogenetics from high-throughput sequencing reads using target enrichment. *Appl. Plant Sci.* **4**. (doi:10.3732/APPS.1600016)

57. Thalén F, Köhne CG, Bleidorn C. 2023 Patchwork: Alignment-Based Retrieval and Concatenation of Phylogenetic Markers from Genomic Data. *Genome Biol. Evol.* **15**. (doi:10.1093/GBE/EVAD227)

58. Madrigal G, Minhas BF, Catchen J. 2024 Klumpy: A tool to evaluate the integrity of

long-read genome assemblies and illusive sequence motifs. *Mol. Ecol. Resour.* , e13982. (doi:10.1111/1755-0998.13982)

59. Quinlan AR, Hall IM. 2010 BEDTools: a flexible suite of utilities for comparing genomic features. *Bioinformatics* **26**, 841–2.

60. Stammnitz MR *et al.* 2023 The evolution of two transmissible cancers in Tasmanian devils. *Science (80-.).* **380**, 283–293. (doi:10.1126/SCIENCE.ABQ6453/SUPPL_FILE/SCIENCE.ABQ6453_MDAR_REPRODUCIBILITY_CHECKLIST.PDF)

61. Ibeh N, Feigin CY, Frankenberg SR, McCarthy DJ, Pask AJ, Romero IG. 2024 De novo transcriptome assembly and genome annotation of the fat-tailed dunnart (Sminthopsis crassicaudata). *GigaByte* **2024**, 35–38. (doi:10.46471/gigabyte.118)

62. Bray NL, Pimentel H, Melsted P, Pachter L. 2016 Near-optimal probabilistic RNA-seq quantification. *Nat. Biotechnol. 2016 345* **34**, 525–527. (doi:10.1038/nbt.3519)

63. Mármol-Sánchez E *et al.* 2023 Historical RNA expression profiles from the extinct Tasmanian tiger. *Genome Res.* **33**, 1299–1316. (doi:10.1101/gr.277663.123)

64. Peel E *et al.* 2022 Genome assembly of the numbat (Myrmecobius fasciatus), the only termitivorous marsupial. *Gigabyte* **2022**, 1–17. (doi:10.46471/GIGABYTE.47)

65. Löytynoja A. 2014 Phylogeny-aware alignment with PRANK. *Methods Mol. Biol.* **1079**, 155–170. (doi:10.1007/978-1-62703-646-7_10)

66. Sela I, Ashkenazy H, Katoh K, acids research TP-N, undefined 2015. 2015 GUIDANCE2: accurate detection of unreliable alignment regions accounting for the uncertainty of multiple parameters. *academic.oup.com* **43**, 7–14. (doi:10.1093/nar/gkv318)

67. Xia X, Xie Z, Salemi M, Chen L, Wang Y. 2003 An index of substitution saturation and its application. *Mol. Phylogenet. Evol.* (doi:10.1016/S1055-7903(02)00326-3)

68. Wertheim JO, Murrell B, Smith MD, Kosakovsky Pond SL, Scheffler K. 2015 RELAX: Detecting Relaxed Selection in a Phylogenetic Framework. *Mol. Biol. Evol.* **32**, 820–832.

69. Yang Z. 2007 PAML 4: Phylogenetic Analysis by Maximum Likelihood. *Mol. Biol. Evol.* **24**, 1586–1591. (doi:10.1093/MOLBEV/MSM088)

70. Wickham H. 2016 ggplot2. (doi:10.1007/978-3-319-24277-4)

71. Anisimova M, Yang Z. 2007 Multiple Hypothesis Testing to Detect Lineages under Positive Selection that Affects Only a Few Sites. *Mol. Biol. Evol.* **24**, 1219–1228. (doi:10.1093/MOLBEV/MSM042)

72. Romiguier J, Figuet E, Galtier N, Douzery EJP, Boussau B, Dutheil JY, Ranwez V. 2012 Fast and robust characterization of time-heterogeneous sequence evolutionary processes using substitution mapping. *PLoS One* (doi:10.1371/journal.pone.0033852)

73. Hubisz MJ, Pollard KS, Siepel A. 2011 Phast and Rphast: Phylogenetic analysis with space/time models. *Brief. Bioinform.* **12**, 41–51. (doi:10.1093/bib/bbq072)

74. Meredith RW, Gatesy J, Murphy WJ, Ryder OA, Springer MS. 2009 Molecular decay of the tooth gene enamelin (ENAM) mirrors the loss of enamel in the fossil record of placental mammals. *PLoS Genet.* **5**. (doi:10.1371/journal.pgen.1000634)

75. Minh BQ, Nguyen MAT, Von Haeseler A. 2013 Ultrafast Approximation for Phylogenetic Bootstrap. *Mol. Biol. Evol.* **30**, 1188–1195. (doi:10.1093/MOLBEV/MST024)

76. Guindon S, Dufayard JF, Lefort V, Anisimova M, Hordijk W, Gascuel O. 2010 New

Algorithms and Methods to Estimate Maximum-Likelihood Phylogenies: Assessing the Performance of PhyML 3.0. *Syst. Biol.* **59**, 307–321. (doi:10.1093/SYSBIO/SYQ010)

77. Minh BQ, Schmidt HA, Chernomor O, Schrempf D, Woodhams MD, Von Haeseler A, Lanfear R, Teeling E. 2020 IQ-TREE 2: New Models and Efficient Methods for Phylogenetic Inference in the Genomic Era. *Mol. Biol. Evol.* **37**, 1530–1534. (doi:10.1093/MOLBEV/MSAA015)

78. Benjamini Y, Speed TP. 2012 Summarizing and correcting the GC content bias in high-throughput sequencing. *Nucleic Acids Res.* **40**, e72. (doi:10.1093/NAR/GKS001)

79. Kim J *et al.* 2022 False gene and chromosome losses in genome assemblies caused by GC content variation and repeats. *Genome Biol.* **23**, 1–29. (doi:10.1186/s13059-022-02765-0)

80. Prieto-Godino LL, Rytz R, Bargeton B, Abuin L, Arguello JR, Peraro MD, Benton R. 2016 Olfactory receptor pseudo-pseudogenes. *Nature* **539**, 93–97. (doi:10.1038/NATURE19824)

81. Nei M, Niimura Y, Nozawa M. 2008 The evolution of animal chemosensory receptor gene repertoires: roles of chance and necessity. *Nat. Rev. Genet. 2008 912* **9**, 951–963. (doi:10.1038/nrg2480)

82. Li WH, Gojobori T, Nei M. 1981 Pseudogenes as a paradigm of neutral evolution. *Nat. 1981 2925820* **292**, 237–239. (doi:10.1038/292237a0)

83. Hara Y, Kuraku S. 2023 The impact of local genomic properties on the evolutionary fate of genes. *Elife* **12**. (doi:10.7554/eLife.82290)

84. Lemos De Matos A, Liu J, McFadden G, Esteves PJ. 2013 Evolution and divergence

of the mammalian SAMD9/SAMD9L gene family. *BMC Evol. Biol.* **13**, 1–16. (doi:10.1186/1471-2148-13-121/FIGURES/7)

85. Meng X, Zhang F, Yan B, Si C, Honda H, Nagamachi A, Sun LZ, Xiang Y. 2018 A paralogous pair of mammalian host restriction factors form a critical host barrier against poxvirus infection. *PLoS Pathog.* (doi:10.1371/journal.ppat.1006884)

86. Liu J, McFadden G. 2015 SAMD9 is an innate antiviral host factor with stress response properties that can be antagonized by poxviruses. *J. Virol.* **89**, 1925–1931. (doi:10.1128/JVI.02262-14)

87. Legrand A *et al.* 2024 SAMD9L acts as an antiviral factor against HIV-1 and primate lentiviruses by restricting viral and cellular translation. *PLOS Biol.* **22**, e3002696. (doi:10.1371/JOURNAL.PBIO.3002696)

88. Li CF *et al.* 2007 Human sterile alpha motif domain 9, a novel gene identified as down-regulated in aggressive fibromatosis, is absent in the mouse. *BMC Genomics* **8**. (doi:10.1186/1471-2164-8-92)

89. Li Q, Guo H, Matsui H, Honda H, Inaba T, Sundberg JP, Sprecher E, Uitto J. 2012 Mouse Samd9l is not a functional paralogue of the human SAMD9, the gene mutated in normophosphataemic familial tumoral calcinosis. *Exp. Dermatol.* **21**, 554–556. (doi:10.1111/J.1600-0625.2012.01524.X)

90. Zhang F, Meng X, Townsend MB, Satheshkumar PS, Xiang Y. 2019 Identification of CP77 as the Third Orthopoxvirus SAMD9 and SAMD9L Inhibitor with Unique Specificity for a Rodent SAMD9L. *J. Virol.* **93**. (doi:10.1128/JVI.00225-19)

91. Matsuda Y, Makino T. 2024 Comparative genomics reveals convergent signals associated with the high metabolism and longevity in birds and bats. *Proc. R. Soc. B*

291. (doi:10.1098/RSPB.2024.1068)

92. Su W, Mao Z, Liu Y, Zhang X, Zhang W, Gustafsson JA, Guan Y. 2019 Role of HSD17B13 in the liver physiology and pathophysiology. *Mol. Cell. Endocrinol.* **489**, 119–125. (doi:10.1016/J.MCE.2018.10.014)

93. Abul-Husn NS *et al.* 2018 A Protein-Truncating HSD17B13 Variant and Protection from Chronic Liver Disease. *N. Engl. J. Med.* **378**, 1096–1106. (doi:10.1056/NEJMOA1712191)

94. Mapes J, Li Q, Kannan A, Anandan L, Laws M, Lydon JP, Bagchi IC, Bagchi MK. 2017 CUZD1 is a critical mediator of the JAK/STAT5 signaling pathway that controls mammary gland development during pregnancy. *PLoS Genet.* **13**. (doi:10.1371/JOURNAL.PGEN.1006654)

95. Fagerberg L *et al.* 2014 Analysis of the human tissue-specific expression by genome-wide integration of transcriptomics and antibody-based proteomics. *Mol. Cell. Proteomics* **13**, 397–406. (doi:10.1074/MCP.M113.035600)

96. Rygiel AM *et al.* 2022 Variants in the pancreatic CUB and zona pellucida-like domains 1 (CUZD1) gene in early-onset chronic pancreatitis - A possible new susceptibility gene. *Pancreatology* **22**, 564–571. (doi:10.1016/J.PAN.2022.04.015)

97. Imamura T, Asada M, Vogt SK, Rudnick DA, Lowe ME, Muglia LJ. 2002 Protection from Pancreatitis by the Zymogen Granule Membrane Protein Integral Membrane-associated Protein-1. *J. Biol. Chem.* **277**, 50725. (doi:10.1074/JBC.M204159200)

98. Van Kooij M, De Groot K, Van Vugt H, Aten J, Snoek M. 2001 Genotype versus phenotype: conflicting results in mapping a lung tumor susceptibility locus to the G7c recombination interval in the mouse MHC class III region. *Immunogenetics* **53**, 656–

661. (doi:10.1007/S00251-001-0381-0)

99. Kumánovics A, Fischer Lindahl K. 2001 G7c in the lung tumor susceptibility (Lts) region of the Mhc class III region encodes a von Willebrand factor type A domain protein. *Immunogenetics* **53**, 64–68. (doi:10.1007/S002510100297)

100. Snoek M, Albertella MR, Van Kooij M, Wixon J, Van Vugt H, De Groot K, Campbell RD. 2000 G7c, a novel gene in the mouse and human major histocompatibility complex class III region, possibly controlling lung tumor susceptibility. *Immunogenetics* **51**, 383–386. (doi:10.1007/S002510050634)

101. Snoek M, Teuscher C, van Vugt H. 1998 Molecular analysis of the major MHC recombinational hot spot located within the G7c gene of the murine class III region that is involved in disease susceptibility. *J. Immunol.* **160**, 266–272.

102. Kachuri L, Francis SS, Morrison ML, Wendt GA, Bossé Y, Cavazos TB, Rashkin SR, Ziv E, Witte JS. 2020 The landscape of host genetic factors involved in immune response to common viral infections. *Genome Med. 2020 121* **12**, 1–18. (doi:10.1186/S13073-020-00790-X)

103. Brennan IG, Keogh JS. 2018 Miocene biome turnover drove conservative body size evolution across Australian vertebrates. *Proc. R. Soc. B* **285**. (doi:10.1098/RSPB.2018.1474)

104. Jiménez-Marín B, Rakijas JB, Tyagi A, Pandey A, Hanschen ER, Anderson J, Heffel MG, Platt TG, Olson BJSC. 2023 Gene loss during a transition to multicellularity. *Sci. Rep.* **13**, 5268. (doi:10.1038/S41598-023-29742-2)

105. Huelsmann M, Hecker N, Springer MS, Gatesy J, Sharma V, Hiller M. 2019 Genes lost during the transition from land to water in cetaceans highlight genomic changes

associated with aquatic adaptations. *Sci. Adv.* **5**, 6671–6696. (doi:10.1126/sciadv.aaw6671)

106. Moeller H. 1970 Vergleichende Untersuchungen zum Evolutionsgrad der Gehirne großer Raubbeutler (Thylacinus, Sarcophilus und Dasyurus). *J. Zool. Syst. Evol. Res.* **8**, 69–80. (doi:10.1111/J.1439-0469.1970.TB00866.X)

107. Dixon JM. 1989 Chapter 20 - Thylacinidae. In *Fauna of Australia* (eds DW Walton, BJ Richardson), pp. 1–36. Canberra: Australian Government Publishing Service.

108. Feigin CY, Newton AH, Pask AJ. 2019 Widespread cis-regulatory convergence between the extinct Tasmanian tiger and gray Wolf. *Genome Res.* **29**, 1648–1658. (doi:10.1101/GR.244251.118/-/DC1)

109. Stern DL. 2013 The genetic causes of convergent evolution. *Nat. Rev. Genet. 2013 1411* **14**, 751–764. (doi:10.1038/nrg3483)

110. Prowse TAA, Johnson CN, Lacy RC, Bradshaw CJA, Pollak JP, Watts MJ, Brook BW. 2013 No need for disease: Testing extinction hypotheses for the thylacine using multi-species metamodels. *J. Anim. Ecol.* **82**, 355–364. (doi:10.1111/1365-2656.12029)

111. De Castro F, Bolker B. 2005 Mechanisms of disease-induced extinction. *Ecol. Lett.* **8**, 117–126. (doi:10.1111/J.1461-0248.2004.00693.X)

112. Paddle R. 2012 The thylacine's last straw: epidemic disease in a recent mammalian extinction. *Aust. Zool.* **36**, 75–92. (doi:10.7882/AZ.2012.008)

113. Seddon PJ, Moehrenschlager A, Ewen J. 2014 Reintroducing resurrected species: selecting DeExtinction candidates. *Trends Ecol. Evol.* **29**, 140–147. (doi:10.1016/J.TREE.2014.01.007)

114. Peers MJL, Thornton DH, Majchrzak YN, Bastille-Rousseau G, Murray DL. 2016 De-extinction potential under climate change: Extensive mismatch between historic and future habitat suitability for three candidate birds. *Biol. Conserv.* **197**, 164–170. (doi:10.1016/J.BIOCON.2016.03.003)

115. Simons M. 2024 Why I work to revive the Tasmanian tiger. *Nature* **631**, 474. (doi:10.1038/D41586-024-02228-5)

116. Wirthlin M, Lovell P V., Jarvis ED, Mello C V. 2014 Comparative genomics reveals molecular features unique to the songbird lineage. *BMC Genomics* **15**, 1–20. (doi:10.1186/1471-2164-15-1082)

117. Paabo S. 1989 Ancient DNA: extraction, characterization, molecular cloning, and enzymatic amplification. *Proc. Natl. Acad. Sci.* **86**, 1939–1943. (doi:10.1073/PNAS.86.6.1939)

118. Sandoval-Velasco M *et al.* 2024 Three-dimensional genome architecture persists in a 52,000-year-old woolly mammoth skin sample. *Cell* **187**, 3541-3562.e51. (doi:10.1016/J.CELL.2024.06.002/ASSET/B94A2BEC-0117-4324-972C-DB0B141C3F23/MAIN.ASSETS/FIGS7.JPG)

119. Tilak MK, Botero-Castro F, Galtier N, Nabholz B. 2018 Illumina Library Preparation for Sequencing the GC-Rich Fraction of Heterogeneous Genomic DNA. *Genome Biol. Evol.* **10**, 616. (doi:10.1093/GBE/EVY022)

120. Spielman D, Brook BW, Frankham R. 2004 Most species are not driven to extinction before genetic factors impact them. *Proc. Natl. Acad. Sci. U. S. A.* **101**, 15261–15264. (doi:10.1073/PNAS.0403809101/SUPPL_FILE/03809TABLE3.PDF)

121. Khan A, Sil M, Thekaekara T, Garg KM, Sinha I, Khurana R, Sukumar R,

Ramakrishnan U. 2024 Divergence and serial colonization shape genetic variation and define conservation units in Asian elephants. *Curr. Biol.* **34**, 4692-4703.e5. (doi:10.1016/J.CUB.2024.08.062)

122. Day EH, Hua X, Bromham L. 2016 Is specialization an evolutionary dead end? Testing for differences in speciation, extinction and trait transition rates across diverse phylogenies of specialists and generalists. *J. Evol. Biol.* **29**, 1257–1267. (doi:10.1111/JEB.12867)

123. Vellend M, Geber MA. 2005 Connections between species diversity and genetic diversity. *Ecol Lett* **8**, 767–781. (doi:10.1111/j.1461-0248.2005.00775.x)

Figure legends

Figure 1. Gene losses in the thylacine (*Thylacinus cynocephalus*). (a) Organs where the lost genes play an important role in the thylacine. We used dog anatomy to illustrate the corresponding organs in the thylacine. (b) Status of the lost genes across 21 marsupial species. A red box indicates gene loss in a given species, while a turquoise box represents an intact gene. The phylogenetic tree used for the analysis was obtained from the TimeTree website (https://timetree.org/) and annotated using iTOL (https://itol.embl.de/). (c) Frame-disrupting events leading to gene loss. The blue box represents intact exons, while the events of exons affected by frame-disrupting changes are shown with yellow highlights. Exons with no BLASTn hits are shown in red, and those with partial BLASTn hits are depicted in orange. Short-read support is shown for four gene-inactivating events of the *SAMD9L* gene (for all events, see electronic supplementary material, figure S2).

Figure 2. The species tree illustrates the gene loss timing in the thylacine lineage, inferred using the 1ds method under the F1x4 codon frequency model in PAML (see electronic

supplementary material, table S6). The mixed branch is coloured in blue, while the functional branches are in black. The yellow-filled rectangle highlights the Middle Miocene Climatic Transition (approximately 15–13 Ma). The time-calibrated phylogeny of Dasyuromorphia and other marsupial species was obtained from the TimeTree website (https://timetree.org/) and annotated in iTOL (https://itol.embl.de/).

Figure 3. The GC content, relaxed selection signatures, and expression analysis of lost genes. (a) Genes classified by TOGA as missing (M), partially missing (PM), partially intact (PI), unclear loss (UL), and clearly lost (L) exhibit high GC content with the prevalence of long stretches of G/C in the thylacine. Vertical and horizontal dotted lines indicate the third quartile values for a particular classification. The lost genes are marked with red-filled triangles and labelled accordingly. (b) Relaxed selection signatures in the thylacine. The x-axis represents the k-value, and the y-axis represents the -log10(p-value) obtained using the RELAX model of HYPHY (see electronic supplementary material, table S5). (c) Heatmap depicting transcript per million (TPM) values of lost genes across tissues. The tissue names and their corresponding SRR IDs are shown on the x-axis. All genes were expressed in at least one tissue above a significant threshold (>1 TPM; see electronic supplementary material, table S4). The plots are generated in R using ggplot2 [70].

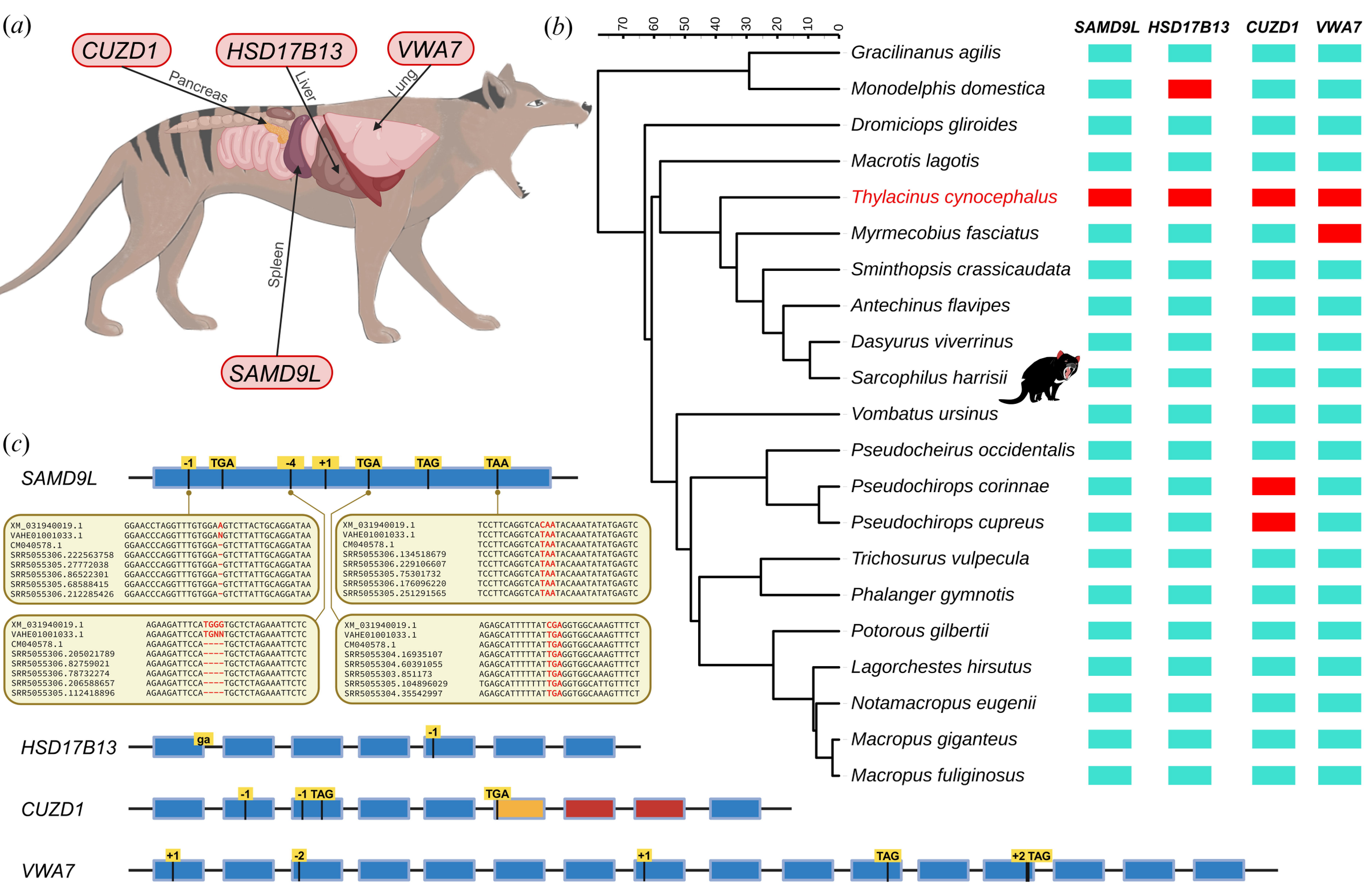
(a)
CUZD1
HSD17B13
VWA7
Pancreas
Liver
Lung
Spleen
SAMD9L
(b)
70
60
50
40
30
20
10
0
SAMD9L
HSD17B13
CUZD1
VWA7
Gracilinanus agilis
Monodelphis domestica
Dromiciops gliroides
Macrotis lagotis
Thylacinus cynocephalus
Myrmecobius fasciatus
Sminthopsis crassicaudata
Antechinus flavipes
Dasyurus viverrinus
Sarcophilus harrisii
Vombatus ursinus
Pseudocheirus occidentalis
Pseudochirops corinnae
Pseudochirops cupreus
Trichosurus vulpecula
Phalanger gymnotis
Potorous gilbertii
Lagorchestes hirsutus
Notamacropus eugenii
Macropus giganteus
Macropus fuliginosus
(c)
SAMD9L
-1
TGA
-4
+1
TGA
TAG
TAA
XM_031940019.1 GGAACCTAGGTTTGTGGAAGTCTTACTGCAGGATAA
VAHE01001033.1 GGAACCCAGGTTTGTGGANGTCTTATTGCAGGATAA
CM040578.1 GGAACCCAGGTTTGTGGA-GTCTTATTGCAGGATAA
SRR5055306.222563758 GGAACCCAGGTTTGTGGA-GTCTTATTGCAGGATAA
SRR5055305.27772038 GGAACCCAGGTTTGTGGA-GTCTTATTGCAGGATAA
SRR5055306.86522301 GGAACCCAGGTTTGTGGA-GTCTTATTGCAGGATAA
SRR5055305.68588415 GGAACCCAGGTTTGTGGA-GTCTTATTGCAGGATAA
SRR5055306.212285426 GGAACCCAGGTTTGTGGA-GTCTTATTGCAGGATAA
XM_031940019.1 TCCTTCAGGTCACAATACAAATATATGAGTC
VAHE01001033.1 TCCTTCAGGTCATAATACAAATATATGAGTC
CM040578.1 TCCTTCAGGTCATAATACAAATATATGAGTC
SRR5055306.134518679 TCCTTCAGGTCATAATACAAATATATGAGTC
SRR5055306.229106607 TCCTTCAGGTCATAATACAAATATATGAGTC
SRR5055305.75301732 TCCTTCAGGTCATAATACAAATATATGAGTC
SRR5055306.176096220 TCCTTCAGGTCATAATACAAATATATGAGTC
SRR5055305.251291565 TCCTTCAGGTCATAATACAAATATATGAGTC
XM_031940019.1 AGAAGATTTCATGGGTGCTCTAGAAATTCTC
VAHE01001033.1 AGAAGATTCCATGNNTGCTCTAGAAATTCTC
CM040578.1 AGAAGATTCCA----TGCTCTAGAAATTCTC
SRR5055306.205021789 AGAAGATTCCA----TGCTCTAGAAATTCTC
SRR5055306.82759021 AGAAGATTCCA----TGCTCTAGAAATTCTC
SRR5055306.78732274 AGAAGATTCCA----TGCTCTAGAAATTCTC
SRR5055306.206588657 AGAAGATTCCA----TGCTCTAGAAATTCTC
SRR5055305.112418896 AGAAGATTCCA----TGCTCTAGAAATTCTC
XM_031940019.1 AGAGCATTTTTATCGAGGTGGCAAAGTTTCT
VAHE01001033.1 AGAGCATTTTTATTGAGGTGGCAAAGTTTCT
CM040578.1 AGAGCATTTTTATTGAGGTGGCAAAGTTTCT
SRR5055304.16935107 AGAGCATTTTTATTGAGGTGGCAAAGTTTCT
SRR5055304.60391055 AGAGCATTTTTATTGAGGTGGCAAAGTTTCT
SRR5055303.851173 AGAGCATTTTTATTGAGGTGGCAAAGTTTCT
SRR5055305.104896029 TGAGCATTTTTTTTGAGGTGGCATTGTTTCT
SRR5055304.35542997 AGAGCATTTTTATTGAGGTGGCAAAGTTTCT
HSD17B13
ga
-1
CUZD1
-1
-1 TAG
TGA
VWA7
+1
-2
+1
TAG
+2 TAG

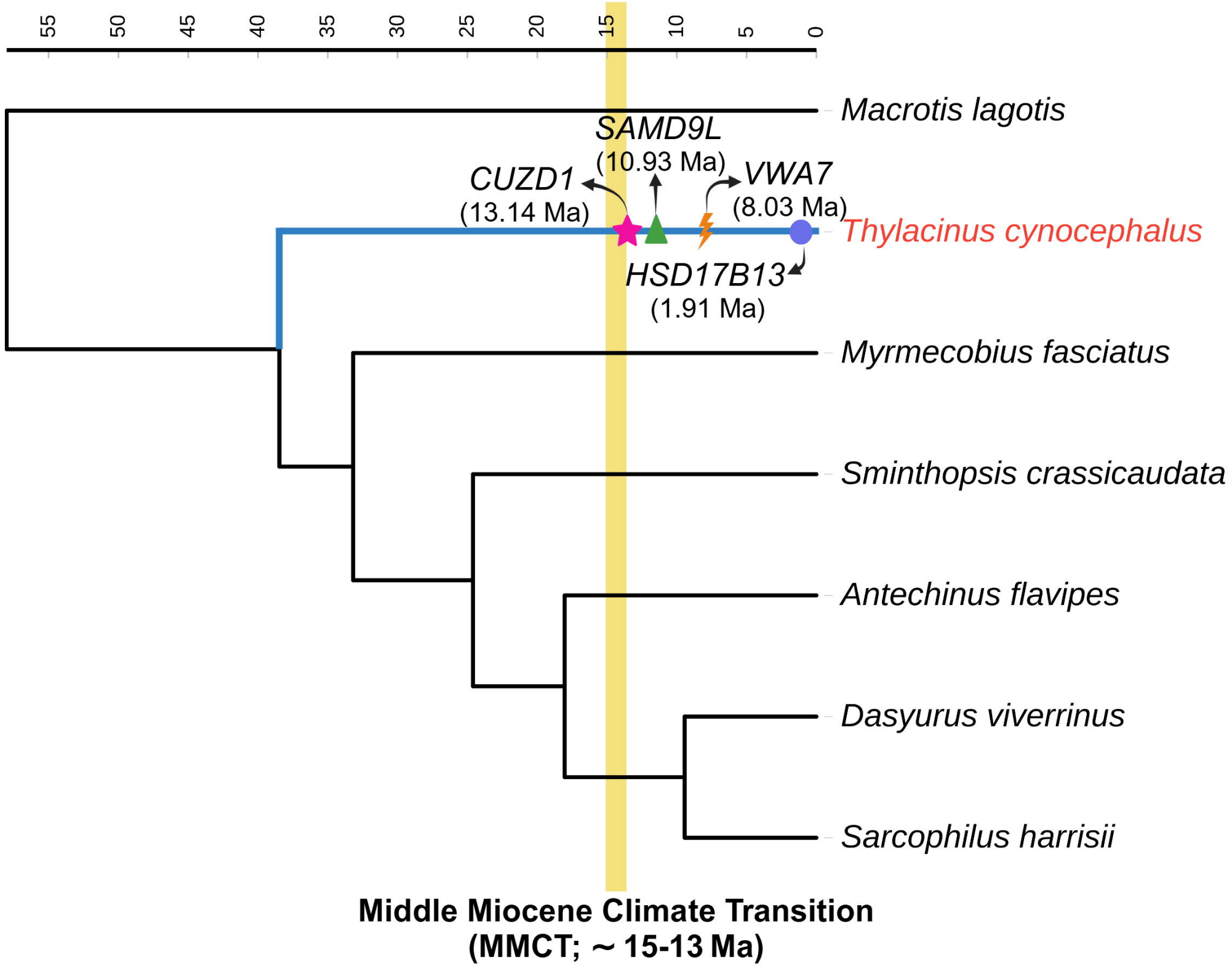
55
50
45
40
35
30
25
20
15
10
5
0
Macrotis lagotis
SAMD9L
(10.93 Ma)
CUZD1
(13.14 Ma)
VWA7
(8.03 Ma)
Thylacinus cynocephalus
HSD17B13
(1.91 Ma)
Myrmecobius fasciatus
Sminthopsis crassicaudata
Antechinus flavipes
Dasyurus viverrinus
Sarcophilus harrisii
Middle Miocene Climate Transition
(MMCT; ~ 15-13 Ma)

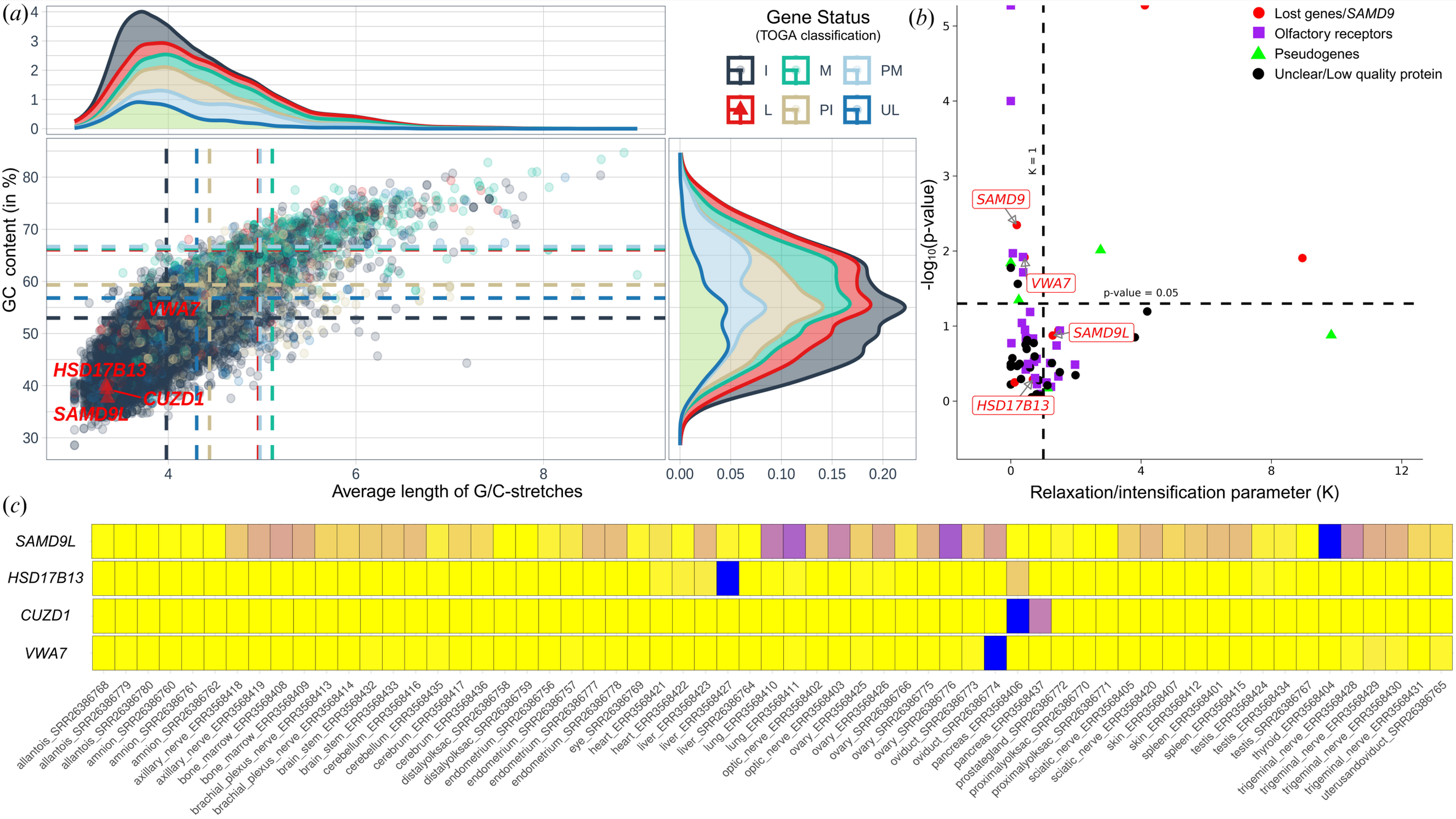
(a)
Gene Status
(TOGA classification)
I
M
PM
L
PI
UL
GC content (in %)
Average length of G/C-stretches
VWA7
HSD17B13
CUZD1
SAMD9L
(b)
Lost genes/SAMD9
Olfactory receptors
Pseudogenes
Unclear/Low quality protein
K = 1
p-value = 0.05
SAMD9
VWA7
SAMD9L
HSD17B13
-log10(p-value)
Relaxation/intensification parameter (K)
(c)
SAMD9L
HSD17B13
CUZD1
VWA7
allantois_SRR26386768
allantois_SRR26386779
allantois_SRR26386780
amnion_SRR26386760
amnion_SRR26386761
amnion_SRR26386762
axillary_nerve_ERR3568418
axillary_nerve_ERR3568419
bone_marrow_ERR3568408
bone_marrow_ERR3568409
brachial_plexus_nerve_ERR3568413
brachial_plexus_nerve_ERR3568414
brain_stem_ERR3568432
brain_stem_ERR3568433
cerebellum_ERR3568416
cerebellum_ERR3568435
cerebrum_ERR3568417
cerebrum_ERR3568436
distalyolksac_SRR26386758
distalyolksac_SRR26386759
endometrium_SRR26386756
endometrium_SRR26386757
endometrium_SRR26386777
endometrium_SRR26386778
eye_SRR26386769
heart_ERR3568421
heart_ERR3568422
liver_ERR3568423
liver_ERR3568427
liver_SRR26386764
lung_ERR3568410
lung_ERR3568411
optic_nerve_ERR3568402
optic_nerve_ERR3568403
ovary_ERR3568425
ovary_ERR3568426
ovary_SRR26386766
ovary_SRR26386775
ovary_SRR26386776
oviduct_SRR26386773
oviduct_SRR26386774
pancreas_ERR3568406
pancreas_ERR3568437
prostategland_SRR26386772
proximalyolksac_SRR26386770
proximalyolksac_SRR26386771
sciatic_nerve_ERR3568405
sciatic_nerve_ERR3568420
skin_ERR3568407
skin_ERR3568412
spleen_ERR3568401
spleen_ERR3568415
testis_ERR3568424
testis_ERR3568434
testis_SRR26386767
thyroid_ERR3568404
trigeminal_nerve_ERR3568428
trigeminal_nerve_ERR3568429
trigeminal_nerve_ERR3568430
trigeminal_nerve_ERR3568431
uterusandoviduct_SRR26386765